*Q. J. R. Meteorol. Soc.* (2000), **126**, pp. 2199–2210

# Empirical forecasts of tropical Atlantic sea surface temperature anomalies

By A. RUIZ DE ELVIRA, M. J. ORTIZ BEVIÁ* and W. CABOS NARVAEZ
*Universidad de Alcalá, Spain*

(Received 26 February 1999; revised 5 November 1999)

SUMMARY

The interannual variability of the tropical Atlantic is characterized by warmings and coolings similar to the Pacific ones (El Niño), and by an interhemispheric signal of decadal variability. The magnitudes of the Gulf of Guinea warmings are less and, therefore, they do not significantly influence the earth's climate, as the El Niño/Southern Oscillation (ENSO) does. In the past, they have been studied because of their connections with the recurrent droughts in the Sahel region. Recently, a number of modelling studies have tried to establish their dependence on ENSO. The real existence of an interhemispheric decadal signal, and its predictability, is also a widely discussed topic. Forecast studies have recently appeared for both the north tropical Atlantic and the Gulf of Guinea regions, and are now operationally available from the National Oceanic and Atmospheric Administration.

In the present work we try first to understand the tropical Atlantic variability in terms of forcings external to the basin. These are identified from 48 years of monthly anomalies of sea surface temperature (SST) data obtained by combining the Comprehensive Ocean and Atmosphere Dataset (COADS) and the Integrated Global Ocean Services System (IGOSS) dataset, and then using the Bayesian theory of estimation. Besides the ENSO-related scales, our analysis retains a decadal time scale in the data variability.

Next, a model is built to forecast the most important features of the equatorial Atlantic interannual variability. These features are monitored through two indices, the Gulf of Guinea and the north tropical Atlantic indices ('the predictands'). Predictor fields are identified from our preliminary analysis, as those time series significantly correlated with the predictands. These correspond to grid points in the tropical Pacific (mainly the Niño3 region, (5°S–5°N, 150°W–90°W)) and tropical Indian oceans. Forecasts were issued for 28 years, at three-monthly intervals. For the north tropical Atlantic index, we have a good forecast skill at leads greater than four months with predictors obtained from east equatorial Pacific time series. For the Gulf of Guinea index, a good forecast skill can be obtained only when we include time series of the equatorial Indian ocean, as well as the east equatorial Pacific, among the predictors. Any of the forecasts presented here show useful forecast skill that, at least, beats persistence at leads greater than four months

KEYWORDS: Predictability Sea surface temperature Statistical methods

## 1. INTRODUCTION

The interannual variability of the tropical Atlantic first attracted attention because of its connection with extreme meteorological events over Africa. The recurrent droughts over the Sahel region and floods in Guinea and Cameroon were related to anomalous sea surface temperatures (SSTs) in the Gulf of Guinea (GG) (Lamb 1978a). Today it is accepted that besides the GG SST, other climatic signals influence the African rainfall. The atmospheric circulation over Africa is also determined by the Indian Ocean SST (Folland *et al.* 1986), and by the dominant global atmospheric signal, the Southern Oscillation (SO) (Nicholson 1986). The spatial characteristics of this variability are well known from the statistical analyses of Wright (1987) and Servain (1991). The anomalies in the equatorial Atlantic are characterized by the GG index. The index is built by averaging SST anomalies in a region (14°S–4°N, 20°W–10°E), represented by a box in Fig. 1.

The behaviour of these indices show that there is not a systematic relationship between the warmings of the Atlantic and the Pacific, as illustrated in Fig. 2(a). The El Niño/Southern Oscillation (ENSO) and the GG warmings were coincidental on three occasions (1951, 1963, and 1968). In four cases the warmings in the Pacific preceded the GG (1963, 1972, 1983, and 1986). On the other hand, the GG warmings of 1967, 1982, and 1991 preceded ENSO, and GG coolings preceded the ENSOs of 1968, 1972, and 1976.

* Corresponding author: Departamento de Física, Universidad de Alcalá, C. Barcelona, Km. 33.6, Alcalá de Henares, Madrid, Spain.

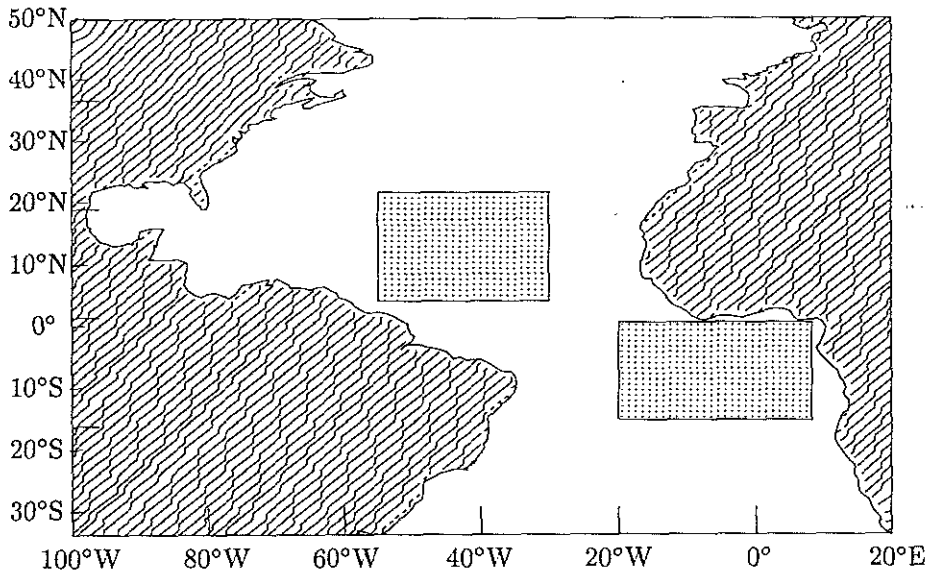


Figure 1. The lower box marks the location of the points whose anomalies were averaged to build the Gulf of Guinea index. The upper box marks the grid points used to build the north Atlantic index.

Observational as well as modelling studies have tried to understand the ENSO–GG warming relationship. For instance, the observational studies of Wagner and Weisberger (1996) and Enfield and Mayer (1997) have shown the connection between ENSO and SST anomalies in the North Atlantic. Also, this relationship has been studied with coupled general-circulation models of the ocean and the atmosphere (Latif and Barnet 1995) and with general-circulation models of the ocean forced with observations (Delecluse *et al.* 1994; Huang and Shukla 1997; Cabos Narvaez *et al.* 1998). In this last work, the GG warmings were monitored through two modes of the heat content of the upper oceanic layers. For the period simulated (the 1980s) the evolution in time of one of these modes is identical to the GG index, while the other closely matches the Niño3 (150°W–90°W, 5°S–5°N) index.

Besides the GG warmings, there is another climatic signal of importance in the tropical Atlantic. This signal has, in the SST anomaly field, the spatial features of a dipole (Servain 1991), and shows important decadal variability. This signal points to anomalies of the interhemispheric gradient: in the first phase, the interhemispheric gradient is weakened, in the other, it is enhanced. This dipole structure appears in statistical analyses of observed Atlantic SST as well as in modelling studies, but while in some studies it seems to have a physical entity (Hastenrath 1978; Chang *et al.* 1997; Wainer and Soares 1997), in others it is considered to be an artefact of the analysis (Houghton and Tourre 1992; Enfield and Mayer 1997; Dommenget and Latif 1998). In fact, such a dipole can be observed sometimes, but it could correspond to a dynamical pattern or be merely the superposition of two independent oscillations, one in the North Atlantic (Latif and Barnett 1995) and the other in the South Atlantic (Venegas *et al.* 1998). The question of the dipole pattern reality is far from being merely an academic issue, because it will show the independence of the Atlantic variability with respect to ENSO, and because of its implications for predictabilty in the Atlantic basin. This issue has been tackled recently in Pendland and Matrosova (1998) with an empirical forecast

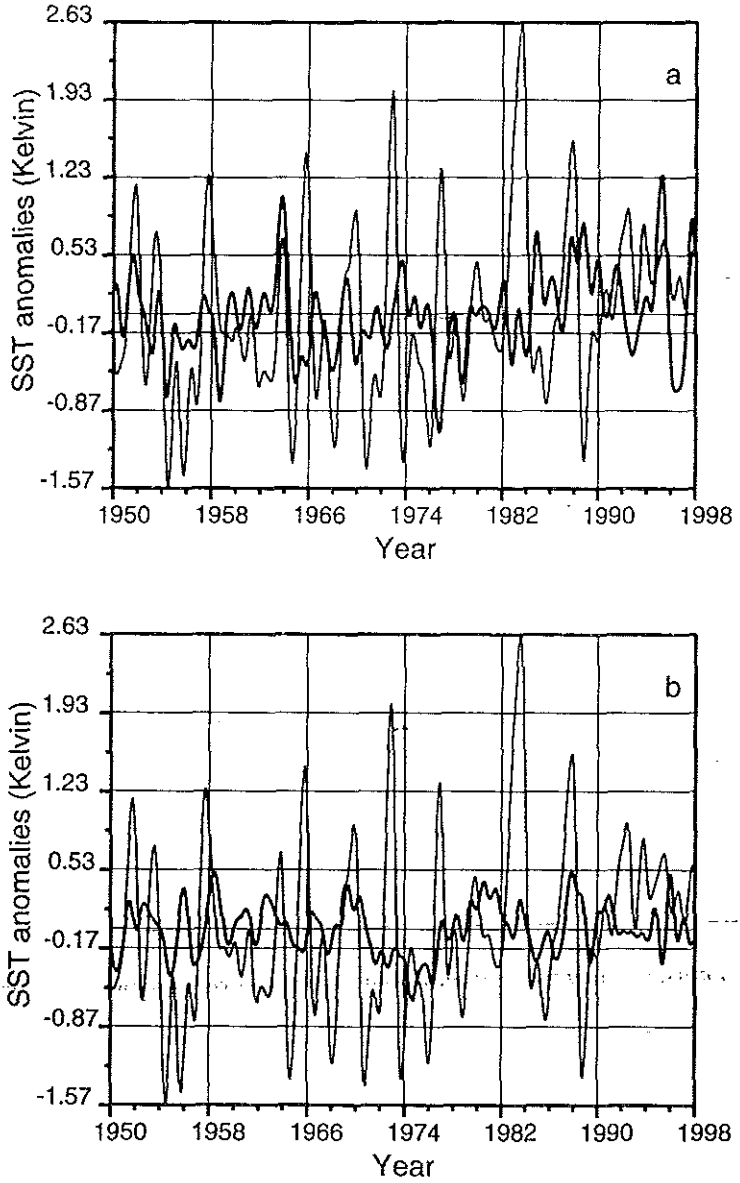


Figure 2. (a): Gulf of Guinea index (thick line) versus the Niño3 (150°W–90°W, 5°S–5°N) index (thin line). (b): North tropical Atlantic index (thick line) versus the Niño3 index (thin line).

model similar to the one routinely used to forecast ENSO (Pendland and Magorian 1993) and their results seem to support the real existence of the tropical Atlantic dipole.

In the present paper, our intention is to contribute to the on-going discussion, with the results of our forecast experiments of the tropical Atlantic anomalous variability, monitored by the GG index and a north tropical Atlantic (NTA) index, using only predictors external to the tropical Atlantic basin. The statistical model used for the forecasts is a slight modification of the one employed by Ruiz de Elvira and Ortiz Beviá (1995) to forecast ENSO. A brief summary is given in section 2. Details of the data and the data treatment used to build the set of predictors as well as the predictands are given

in section 3. In section 4 we explain the layout of the forecast experiments and their results. These results are discussed in section 5.

## 2. Statistical model: Bayesian oscillation patterns

We want to understand the quasi-periodical evolution of the SST in the tropical Atlantic as a superposition of a small number of spatial patterns, each oscillating with a fixed frequency.

Let us collect our $s$ observations of a physical variable on the $n$ points of a grid, into $s$ realizations of a $n$ dimensional vector, $\mathbf{d}(t_i)$, $i = 1, \ldots, r$. A suited average of some of these components will be called an index $I(t_i)$, while some other components will form the predictor field: $p_j(t_i)$, $j = 1, \ldots, N$; $i = 1, \ldots, s$. We want to issue forecasts for $t_k$, $k = s + 1, \ldots$.

We would like to understand the observations in terms of a model

$$m(t_i) = \sum_{v=1}^{N} a_v G_v\{t_i; (\omega)\} \tag{1}$$

where $\omega$ is the set of parameters of the model, and $m$ the one-dimensional model representing the index. The $N$ spatial coefficients, $a_v$, will be called patterns. The $N$ functions, $G_v$, are the time-frequency a priori model functions.

The parameters, $\omega$, will be determined as the most probable time-scales using the Bayesian theory of estimation. Bayes theorem allows us to write the probability that some data, $\mathbf{d}$, can be described by a model, $M$, given some previous information, $\mathcal{I}$, as

$$P(M|\mathbf{d}, \mathcal{I}) = \frac{P(M|\mathcal{I})P(\mathbf{d}|M, \mathcal{I})}{P(\mathbf{d}|\mathcal{I})}. \tag{2}$$

The posterior probability we are looking for, $P(M|\mathbf{d}, \mathcal{I})$, is then the product of the prior probability of the model, $M$, given information, $\mathcal{I}$, $P(\mathbf{d}|\mathcal{I})$, and of $P(\mathbf{d}|M, \mathcal{I})$, the probability of finding the data given a model, $M$. If we stick to the most uninformative probability for the sequence $w_{t_1}, w_{t_2}, \ldots, w_{t_m}$, we will have

$$P(\mathbf{d}|M, \sigma, \mathcal{I}) = \prod_{i=1}^{r} \left\{ \frac{1}{\sqrt{2\pi\sigma^2}} \exp\left( -\frac{(\mathbf{d}_{t_i} - m_{t_i})^2}{2\sigma^2} \right) \right\} \propto \sigma^{-r} \exp\left( -\frac{\sum_{i=1}^{r} (\mathbf{d}_{t_i} - m_{t_i})^2}{2\sigma^2} \right) \tag{3}$$

that has, in this case, the same mathematical expression as the likelihood used in the classical theory of estimation, and where $\sigma$ is the standard deviation of the data.

Bayesian inference (Jeffreys 1961) is nevertheless quite different from the classical one. While the mathematical expression that gives the probability is the same, its functional dependence is not. In the classical theory, we have to estimate the parameters of our model because we are given only a 'sample'; if we had the whole population we could determine their true value. With our 'sample' data we can only 'estimate' a value for these parameters (by maximizing the likelihood Eq. (3), for instance) together with a confidence interval at the chosen level of significance. The accuracy of our estimated value depends greatly on the estimation hypothesis being satisfied, for instance, residuals need to be gaussian and uncorrelated, etc.

In the Bayesian theory of estimation, parameters are stochastic variables and, therefore, do not have a 'true value'. We can test any possible value of the parameters that we can imagine, and we will have a probability for each value. Therefore, because

the hypotheses are less restrictive, Bayesian estimation can ignore the characteristics of residuals, etc. while classical estimation cannot.

Coming now to the practical procedure, let $\{I(t_i), t_i = 1, \ldots, s\}$ be our predictand field (that is, the index we want to forecast) and let $\{p_j(t_i); j = 1, \ldots, N; t_i = 1, \ldots, s\}$ be our predictor field (the $N$ time series we will use as predictors). Let $t_k, k = 1, \ldots, s$ be the times used for the learning sample to issue a forecast for the times $t_k, k = s + 1, \ldots, M$.

First, and for each predictor, once the $q$ basic time-scales have been identified by the procedure described above, we compute an orthonormal basis from the a priori $\{G_\mu(t_i), \mu = 1, q\}$ functions:

$$H_\nu(t_i) = \sum_{\mu=1}^{q} C_{\nu\mu} G_\mu(t_i) \tag{4}$$

where $C_{\nu\mu}$ is the matrix of the change of basis, and where $H_\nu(t_i)$ satisfy

$$\sum_{i=1}^{s} H_\nu(t_i) H_\mu(t_i) = \delta_{\nu\mu} \tag{5}$$

where $\delta_{\nu\mu}$ is the Dirac delta function, and we project the predictors, $p_j(t_i)$, onto this orthonormal basis

$$b_{\nu j} = \sum_{i=1}^{s} p_j(t_i) H_\nu(t_i) \tag{6}$$

forming a new series of a priori functions, $fg_\nu(t_i), \nu = 1, \ldots, N; i = 1, \ldots, s$, from the coefficients, $b$, and the original functions, $G$.

The eigenvectors of the covariance matrix, $\Xi$,

$$\Xi = \sum_{i=1}^{s} \sum_{\nu=1}^{q} fg_{\nu j}(t_i) fg_{\nu k}(t_i) \tag{7}$$

between these functions, $fg$, provide a new spatial basis, $(z_{jl}, j, l = 1, N)$, onto which we project $fg_{\nu j}(t)$, obtaining the final functions, $hg(t)$.

$$hg_j(t_i) = \sum_{k=1}^{n} fg_k(t_i) z_{kj}; \; j = 1, \ldots, q. \tag{8}$$

From these $N$ predictors we will only choose the $q$ ones for which the probabilities are maxima.

The correlation between the predictand, $p(t_i)$, and these coefficients, $hg_j$, for the length of the learning interval yields some spatial coefficients, $c$:

$$c_j = \sum_{i=1}^{s} p(t_i) hg_j(t_i), \tag{9}$$

that will allow us to issue a forecasted time series, $I(t_i)$, for the predictand at times $t_i = s + 1, \ldots, N$,

$$I(t_i) = \sum_{j=1}^{q} c_j hg_j(t_i); \; i = s + 1, \ldots . \tag{10}$$

## 3. DATA AND DATA TREATMENT

To build our predictor dataset we used two sources of data. Monthly means of observations of SST anomalies from the Comprehensive Ocean and Atmosphere Dataset (COADS, Woodruff *et al.* 1987) cover the period from 1950 through to 1993. The data are global, in a grid size ($2° \times 2°$) in longitude and latitude. The Integrated Global Ocean Services System (IGOSS) dataset, which includes data from ships and buoys and bias corrected data from satellites, goes from 1982 through to 1997. These data are global, in a grid size ($1° \times 1°$). For our merged field we will use the COADS grid specification. Therefore, the IGOSS data will be interpolated onto the COADS grid. For each COADS grid point in the centre of a square, we will average the IGOSS observation at the square vertices, and the point at the centre. The final data are no more statistically dependent than the original gridded data were.

Finally, those points without enough observations in time were suppresed. In the remaining time series the time points without data were filled with the monthly mean values from the series plus a small random number. No interpolation in time was performed.

Monthly mean averages for the period 1950–1997 were estimated and subtracted from each value. Afterwards, the anomalous time series were filtered in time, removing the variability corresponding to time-scales shorter than ten months.

## 4. ANALYSIS OF THE FORECAST-EXPERIMENTS

The a priori functions selected for the analysis were ($\cos(\omega t)$, $\sin(\omega t)$, $\cos^3(\omega t)$, $\sin^3(\omega t)$). The $\omega$ are the frequencies corresponding to the five more probable characteristic time-scales. For the prediction for the North Atlantic, 180 time series in the Pacific, in a region from 80°W to 130°W and from 12°S to 12°N, were used.

For the prediction of the GG index, 412 time series were used. From these, 202 were in the Indian Ocean, from the Madagascar coast to the south of Sri Lanka, and 210 were in the east Pacific, mostly in the Niño3 region.

From these, the spatial coefficients were computed, and from these predictors only $q = 30$ were taken into account for our forecast, where $q$ is determined as explained in section 2.

Our forecasting scheme can be summarized as follows:

- An automatic procedure selects the most important characteristic time-scales—CTSs—(up to a number of five) for the predictor time series, for the times between $t_0$ (the start of the series, January 1950) and $t_i$ (the start of forecast, in this case, from January 1970 until October 1997, at three-monthly intervals).
- With these CTSs and the a priori functions, a subsequent procedure optimizes the fit for the length of the training period.

The ability to forecast is frequently measured by the skill of correlation defined as:

$$S_\tau = \frac{\sum_{t_{i_i}+\tau}^{t_{i_f}+\tau} y(t_i+\tau) y_m(t_i+\tau)}{\sqrt{\left\{\sum_{t_{i_i}+\tau}^{t_{i_f}+\tau} y^2(t_i+\tau)\right\}\left\{\sum_{t_{i_i}+\tau}^{t_{i_f}+\tau} y_m^2(t_i+\tau)\right\}}} \qquad (11)$$

where $t_{i_i}$ are the different initial times for the starts of forecasts, and $t_{i_f}$ are the different final times we can use. $\tau$ is the number of months we want to forecast. For instance, $t_i$ varies in our case from $t_{i_i} = 480$ months to $t_{i_f} = 550$ months.

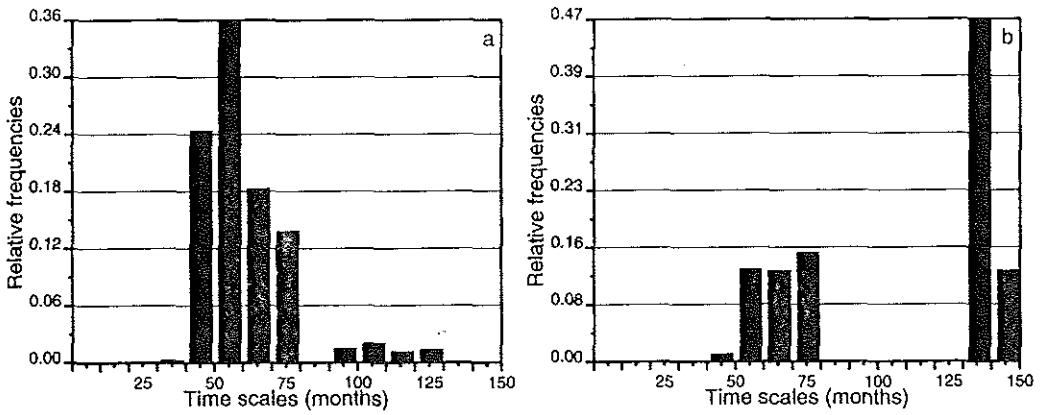


Figure 3. Characteristic time-scales selected for the forecasts for the 1990s. (a): Gulf of Guinea index. (b): North tropical Atlantic index.

In this way, for each forecast, the CTS can be different, and indeed they do vary slightly. Nevertheless, if we represent in a histogram all the CTSs selected for the experiments performed during the 1990s, we can see that the selected CTSs are roughly the same, and what varies is the importance of a CTS (its weight) in each forecast. Then, for instance, in the histogram of Fig. 3(a), which represents the CTSs selected to forecast the NTA index, we can see that the selected CTSs fall into two, well separated, groups, one that corresponds to the three ENSO time-scales and the other, more importantly, to the decadal time-scales. In the histogram representing the CTSs used for the GG index forecasts (Fig. 3(b)), only the ENSO related time-scales are important, while the decadal scale is irrelevant.

The procedure used to forecast is different from the one used in other empirical or dynamical predictions. Given the point of the start of a forecast, we simply reconstruct our predictand time series using the a priori functions up to the time we want to forecast. The forecasted values at $\tau$ units of time after the start of our forecast will be used to compute the skill for this $\tau$ lead.

Our Fig. 4(b) shows the skill of our 108 forecasting experiments of the NTA index (represented with a solid line) against the skill given by persistence (that is the forecasted value equal to the one last observed), represented with a dashed line. In the top panel we do likewise for the GG index. These values of the skill have to be assessed against the confidence levels of the zero value for the correlation at the 95% significance level, which for $M$ greater than 60 will be given (up to the second decimal place) by $S_s = 2/\sqrt{M}$, where $M$ is the number of elements in the sums defining the correlation (i.e. in this case, the number of initial times for the forecasts). Because the number of predictors is not small we have to consider values of the artificial skill. We take as an estimation of the artificial skill (Davis 1976), the expression $S_a = (n/M)(\tau/\delta t)$, where $n$ is the number of predictors, $\delta t$ the forecast-time sampling scale and $\tau$ a characteristic time-scale determined by the product of the auto-covariances of both predictor and predictand fields. In the present case, for the forecasts for the 1970s–1990s, $S_s = 0.2$ and $S_a = 0.4$, while for the 1990s' forecasts, $S_s = 0.3$ and $S_a = 0.6$. In both cases, these values are below the skill of our forecasts, as shown by our Fig. 4.

Additionally, a common-sense rule, usually applied, says that a useful forecast must have a correlation skill above 0.6. As we can see (Fig. 4(b)), our forecasts of the NTA index for the period 1970–1997 beat persistence for time leads greater than three months

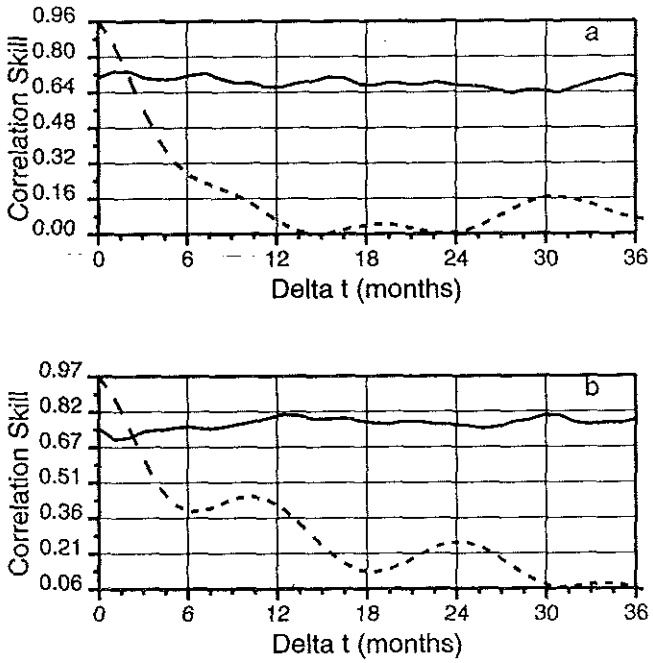


Figure 4. The 1970s, 1980s and 1990s. (a): correlation skill for the forecast of the Gulf of Guinea index with predictors from the Atlantic sea surface temperature (SST). (b): correlation skill for the forecast of the north tropical Atlantic index using the tropical Pacific SST predictors. The dashed lines represent the skill given by persistence.

and remain useful for time leads up to 24 months. After an initial decrease in the skill, there is an increase from four months to one year, after which the skill steadily decreases until 26 months. The forecast of the GG index for the same period, using only tropical Atlantic predictors, shows similar values of skill. There are, nevertheless, some differences.

Our GG index forecast beats persistence skill earlier, and shows better values for shorter leads. In Fig. 5 we represent the skill of our forecasts of the GG index of the 1990s (bottom panel) using predictors determined with only Pacific and Indian time series. At shorter leads, values of the skill are below those obtained with only Atlantic predictors, while at longer leads they are better. There is no remarkable difference between the behaviour and values of the skill of our forecasts in the 1990s and those obtained for the whole period (predictors in both cases are identified from the same equatorial Pacific time series).

As an illustration of the performance of our forecast, we have represented in Fig. 6 the NTA index from observations (thin line) versus our forecasts for two different leads. As indicated by the correlation skill, the general performance is satisfactory, though the magnitude of the anomalies is underestimated. An exceptional period is the sustained cooling during the 1970s, which is not well predicted. The forecasted variability for this period is better at the longer lead.

The same behaviour can be observed for the GG index reconstructed from our forecasts. In this case, a localized cooling event appears in 1977, and is missed by all our forecast experiments. In our Fig. 7 we show the GG index from observations (with a thin line) versus our forecasts using Pacific+Indian predictors, represented with a thick line.

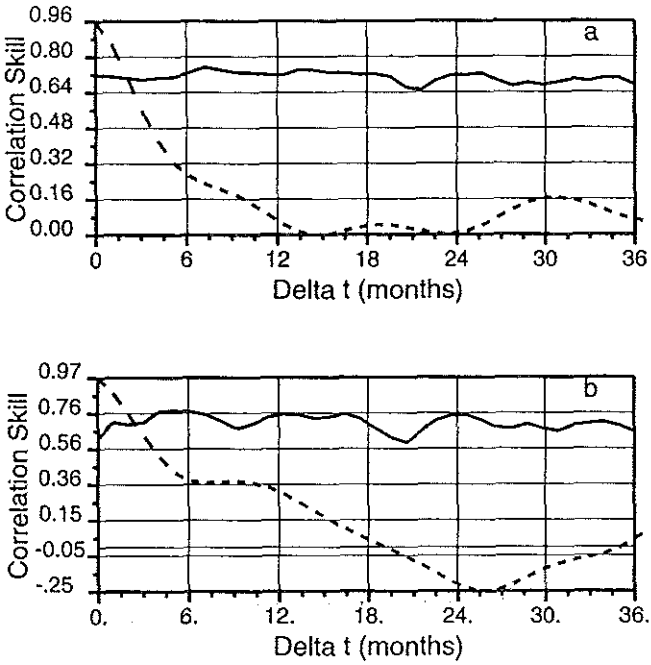


Figure 5. (a): Correlation skill for the forecast of the Gulf of Guinea index using Indian and Pacific sea surface temperature (SST) anomalies as predictors, for the 1970s, 1980s and 1990s. (b): Correlation skill for the forecast of the Gulf of Guinea index using Indian and Pacific SST anomalies as predictors, for the 1990s. The dashed lines represent the skill given by persistence.

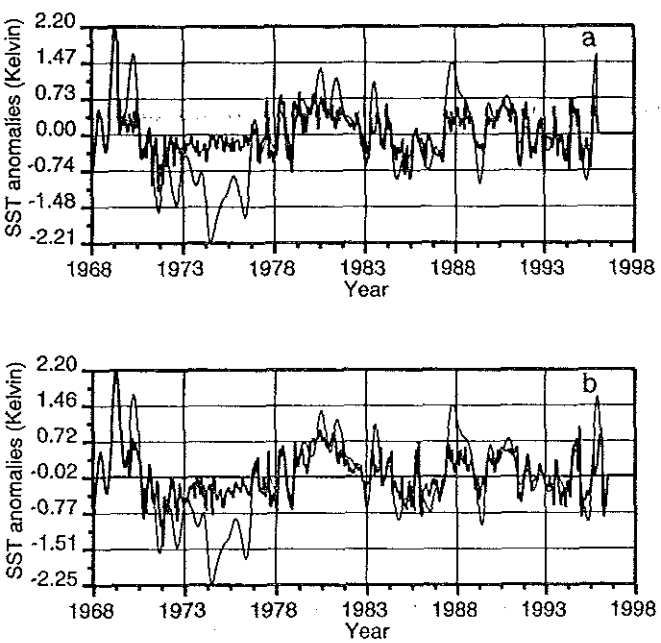


Figure 6. (a): We represent our forecast for two seasons in advance of the north tropical Atlantic index (thick line) versus the values determined from observations (thin line). In (b) we do likewise for the forecast one year in advance.

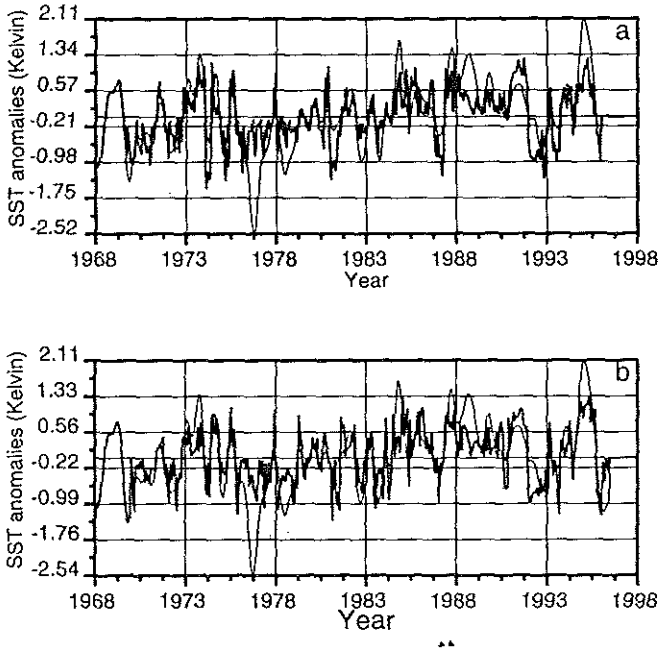


Figure 7. (a): We represent our forecast for two seasons in advance of the Gulf of Guinea index (thick line) versus the values determined from observations (thin line). In (b) we do likewise for the forecast one year in advance. Both forecasts use the Indian and tropical Pacific predictors.

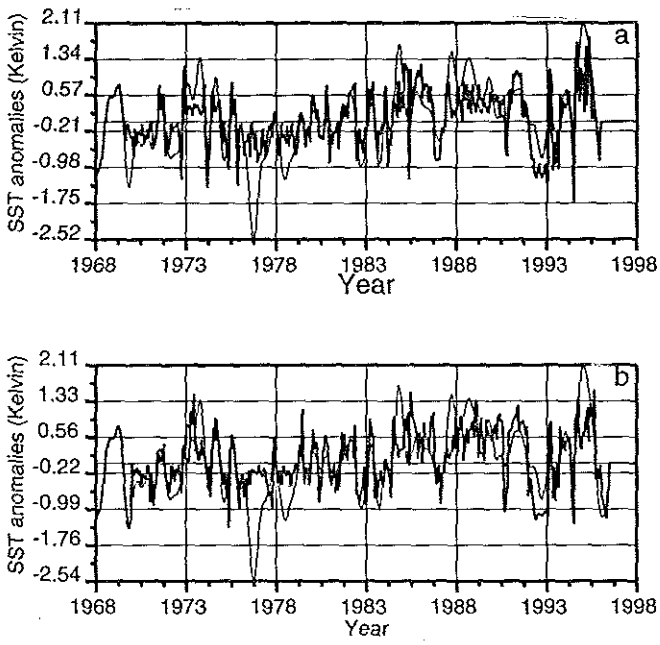


Figure 8. (a): We represent our forecast for two seasons in advance of the Gulf of Guinea index (thick line) versus the values determined from observations (thin line). In (b) we do likewise for the forecast one year in advance. Both forecasts use the Atlantic predictors.

In Fig. 8 we represent the same indices but for forecasts made with Atlantic predictors. The magnitude of the anomalies seems to be better estimated in this case.

## 5. Discussion

A simple statistical model, the Bayesian oscillation pattern, was applied here to the prediction of the anomalous variability of the tropical Atlantic. The variability of the tropical Atlantic is characterized by two indices, the NTA index and the GG index. In previous work, the model was set successfully to forecast ENSO events. In the work reported here, the model proves valuable: The skill of our forecasts of both indices is good and beats persistence skill for time leads greater than roughly one season. In any case, the model forecasts have distinctive features which are better than the persistence forecasts, such as their ability to forecast the start of the anomalous warming or cooling events in the Gulf of Guinea.

There are several additional interesting features in our forecasts. In two out of the three experiments, the predictors lay outside the Atlantic basin. In order to have successful forecasts of the NTA, predictors can be identified with time series of the Niño3 region. For the GG index, an acceptable skill value can be achieved only when additional observations from the tropical Indian Ocean are included. In our third set of experiments, forecasts are performed for the GG index with predictors identified from observations of the tropical Atlantic. The skills of our forecasts of the GG index, in our second and third experiments, are similar, but those with Atlantic predictors perform better at leads up to eight months.

Further insight can be obtained from the distribution of the most frequent time-scales selected to forecast the 1990s. In the case of the NTA, these are dominated by decadal ones, while the decadal time-scale is not important for the GG forecasts. This distribution helps us to understand why the GG index forecasts, with Atlantic predictors, have better skill at shorter leads, and why the skill recovers at longer leads when this index is forecasted with predictors that include Pacific grid points.

These results seem to point in the same direction as the other studies already mentioned: That the anomalous variabilities in the north and south tropical Atlantic are not connected, and the dipole pattern associated with the decadal variability is an artefact of the analysis. It seems intriguing that the dipole pattern always appears when the spatial coherence is taken into account (as in an analysis in terms of empirical orthogonal functions), and that when only the time-evolution features are considered, the decadal time-scale is not important in the equatorial Atlantic. In any case, the picture emerging out of this analysis is not inconsistent with our previous findings: The influence of the NTA in the GG events is due to ENSO events.

The reconstruction of both indices at different leads allows further comparative studies. There is a cooling in the NTA index, of decadal characteristics, which our forecast misses. Nevertheless, it is better captured in the forecasts with longer lead times. The same feature can be observed in the GG index, where the cooling has localized characteristics. Some complementary forecast experiments for the 1970s, already underway, might help us to understand the relationships between the north and south regions of the tropical Atlantic.

## Acknowledgement

This work was supported by the European Union Environment and Climate Programme under contract CT95-0109.

## REFERENCES


Cabos Narvaez, W. D., Ortiz Beviá, M. J. and Oberhuber, J. M. 1998 The tropical Atlantic variability. *J. Geophys. Res.*, **103**, 7475–7489

Chang, P., Ji, L. and Li, H. 1997 A decadal climate variation in the tropical Atlantic Ocean from thermodynamics of air–sea interactions. *Nature*, **385**, 516–518

Davis, R. E. 1976 Predictability of sea surface temperature and sea level pressure anomalies over the North Pacific Ocean. *J. Phys. Oceanogr.*, **6**, 249–266

Delecluse, P., Servain, J., Levy, C., Arpe, K. and Bengtsson, L. 1994 On the connection between the 1984 Atlantic warm event and the 1982–1983 ENSO. *Tellus*, **A 4**, 448–464

Dommenget, D. and Latif, M. 1981 'Interannual to decadal variability in the tropical Atlantic'. Max Planck Institut für Meteorologie Report, Hamburg

Endfield, D. B. and Mayer, D. A. 1997 Tropical Atlantic sea surface temperature and its relation to El Niño-Southern Oscillation. *J. Geophys. Res. Lett.*, **23**, 929–945

Folland, C. K., Owen, J. A., Ward, M. N. and Colman, A. W. 1991 Prediction of seasonal rainfall in the Sahel region using empirical and dynamical methods. *J. Forecasting*, **10**, 21–56

Hastenrath, S. 1978 On modes of tropical circulation and climate anomalies. *J. Atmos. Sci.*, **35**, 2222–2231

Huang, B. and Shukla, J. 1997 A numerical simulation of the variability in the tropical Atlantic Ocean. *J. Phys. Oceanogr.*, **27**, 1693–1712

Houghton, R. W. and Tourre, Y. M. 1992 Characteristics of low frequency sea surface temperature fluctuations in the Tropical Atlantic. *J. Climate*, **5**, 765–771

Jeffreys, H. 1961 *Theory of probability*. Oxford University Press, Oxford, UK

Lamb, P. J. 1978 Large scale tropical surface circulation patterns during recent sub-Saharian weather anomalies. *Tellus*, **30a**, 240–251

Latif, M. and Barnett, T. P. 1995 Interactions of the Tropical Oceans. *J. Climate*, **8**, 952–964

Moron, A. and Fontaine, B. 1996 Sahel droughts and ENSO dynamics. *J. Geophys. Res. Lett.*, **23**, 515–518

Nicholson, S. E. 1986 The quasiperiodic behaviour of rainfall variability in Africa and its relationships with the SO. *Arch. Met. Geoph. Biocl., Ser. A*, **34**, 311–348

Pendland, C. and Magorian, T. 1993 Prediction of Niño3 sea surface temperature using linear inverse modeling. *J. Climate*, **6**, 1067–1076

Pendland, C. and Matrosova, L. 1998 Prediction of tropical Atlantic sea surface temperature using linear inverse modeling. *J. Climate*, **11**, 483–496

Ruiz de Elvira, A. and Ortiz Beviá, M. J. 1995 Application of statistical techniques to the analysis and prediction of ENSO. *Dyn. Atmos. Oceans*, **22**, 91–114

Servain, J. 1991 Simple climatic indices for the tropical Atlantic Ocean and some applications. *J. Geophys. Res.*, **96**, 15137–15146

Venegas, S., Mysak, L. and Straub, D. 1998 An interdecadal climate cycle in the South Atlantic and its links to other ocean basins. *J. Geophys. Res.*, **103**, 24723–24736

Wagner, T. J. and Weisberger, R. H. 1996 Mechanisms controlling variability of the interhemispheric sea surface temperature gradient in the tropical Atlantic. *J. Climate*, **9**, 2010–2019

Wainer, I. and Soares, J. 1997 North northeast Brazil rainfall and its decadal-scale relationship to wind stress and sea surface temperature. *J. Geophys. Res. Lett.*, **24**, 277–280

Woodruff, S. D., Slutz, R. J., Jenne, R. L. and Steurer, P. M. 1987 A comprehensive ocean–atmosphere data set. *Bull. Am. Meteorol. Soc.*, **68**, 1239–1250

Wright, E. B. 1987 'Variations in the tropical Atlantic sea surface temperature and their global relationships.' M.P.I.M. Report, 12